A&A 486, 493–496 (2008)
DOI: 10.1051/0004-6361:200809851

Astronomy & Astrophysics

Limits on chemical complexity in diffuse clouds: search for CH_3OH and HC_5N absorption⋆

H. S. Liszt[1], J. Pety[2,3], and R. Lucas[2]

[1] National Radio Astronomy Observatory, 520 Edgemont Road, Charlottesville, VA, 22903-2475, USA
e-mail: hliszt@nrao.edu
[2] Institut de Radioastronomie Millimétrique, 300 rue de la Piscine, 38406 Saint Martin d'Hères, France
[3] Obs. de Paris, 61 Av. de l'Observatoire, 75014 Paris, France

Received 26 March 2008 / Accepted 10 May 2008

ABSTRACT

Context. An unexpectedly complex polyatomic chemistry exists in diffuse clouds, allowing detection of species such as C_2H, C_3H_2, H_2CO, and NH_3, which have relative abundances that are strikingly similar to those inferred toward the dark cloud TMC-1.
Aims. We probe the limits of complexity of diffuse cloud polyatomic chemistry.
Methods. We used the IRAM Plateau de Bure Interferometer to search for galactic absorption from low-lying J = 2–1 rotational transitions of A- and E-CH_3OH near 96.740 GHz and used the VLA to search for the J = 8–7 transition of HC_5N at 21.3 GHz.
Results. Neither CH_3OH nor HC_5N were detected at column densities well below those of all polyatomics known in diffuse clouds and somewhat below the levels expected from comparison with TMC-1. The HCN/HC_5N ratio is at least 3–10 times higher in diffuse gas than toward TMC-1.

Key words. ISM: molecules – astrochemistry – ISM: clouds

1. Introduction

As we have shown in a recent series of papers, local diffuse clouds seen in cm-wave and mm-wave absorption against extragalactic background sources have an unexpectedly rich and robust polyatomic chemistry (see Liszt et al. 2006 and references given there). At lower column densities CO, OH, HCO^+, C_2H and C_3H_2 are detected but when $N(HCO^+) \gtrsim 10^{12}$ cm^{-2} or $N(H_2) \gtrsim 5 \times 10^{20}$ cm^{-2}, CS, HCN, NH_3 and H_2CO appear with relative abundances like those inferred toward the canonical dark cloud TMC-1 (Ohishi et al. 1992).

Some fairly complex species are seen in these absorption studies, but the real limits of complexity within this chemistry are not known. Most of our work has been at mm-wavelengths while larger astrophysically-important species are generally heavier so that the bulk of their rotational population resides in energy levels which are best observed at lower frequencies.

An exception to this general scenario is methanol (CH_3OH), many of whose lowest rotational transitions (including the ground-state E-type transition) occur near 96 740 MHz. These lines were detected in TMC-1 by Friberg et al. (1988) and the relative abundance of CH_3OH with respect to HCO^+ in TMC-1 is $N(CH_3OH)/N(HCO^+) \approx 0.25$ (Ohishi et al. 1992). Although the generally-accepted chemical scheme for producing methanol in dark gas invokes progressive hydrogenation of H_2CO on grains and might not be expected to be a fertile source of molecules in lightly-shielded regions, H_2CO is widely seen in diffuse clouds (Nash 1990; Liszt & Lucas 1995; Liszt et al. 2006). Furthermore, the environment is rich in atomic hydrogen in diffuse gas and models have been proposed in which molecules are hydrogenated on grains and released into the ambient diffuse gas where high abundances persist for some time (Viti et al. 2000; Price et al. 2003). Alternatively, material may be cycled through a dense phase, with persistently high molecular abundances for quite some time thereafter in a more diffuse state (Falgarone et al. 2006). This being the case, at the suggestion of our colleagues, we undertook to search for CH_3OH absorption using the IRAM Plateau de Bure Interferometer.

An alternative approach to searching for heavier molecules is simply to follow them to lower frequencies and, subsequent to the CH_3OH observations described here, we realized that the cyanopolyynes HC_3N and HC_5N should be observable with high sensitivity during the VLA-eVLA conversion. Given the similarity in abundance between so many species in TMC-1 and diffuse gas, and the high relative abundances of the cyanopolyynes in TMC-1 (where N(HCN):N(HC_3N):N(HC_5N) = 20:6:3) it seemed appropriate to search for just those species which are the particular hallmark of the chemistry in TMC-1.

Section 2 of this work describes the observations and some aspects of the spectroscopy of CH_3OH. Section 3 describes the cyanopolyyne work and Sect. 4 presents our upper limits on the CH_3OH and HC_5N abundances and briefly summarizes our absorption line work to date as well as the physical conditions under which the diffuse cloud chemistry operates.

2. CH_3OH observations and data

2.1. Observed sources and technical details

The data were acquired at the Plateau de Bure Interferometer in May and July 2006 with 5 or 6 antennas. Table 1 summarizes the observed sightlines, observing dates, approximate quasar fluxes, integration times (the on-source time equivalent

⋆ Based on observations obtained with the IRAM Plateau de Bure Interferometer and the NRAO VLA telescope.

Table 1. Background sources observed in CH_3OH .

Source	l °	b °	Date 2006	Flux Jy	Time hours[2]	$\sigma^1_{l/c}$ $\times 10^{-3}$
B0355+508	150.4	−1.6	July	2.8	3.5	8.5
B0415+379	161.7	−8.8	July	2.6	4.2	14.5
B2200+420	92.6	−10.4	May	2.5	8.2	6.5

[1] $\sigma_{l/c}$ = rms error in the line/continuum ratio; [2] Integration time on-source equivalent to using 6 antennas.

Table 2. CH_3OH spectroscopy and column density.

Line	ν MHz	A_{21} 10^{-6} s^{-1}	$f^1_{\rm low}$	q^2 cm^{-2}/km s^{-1}
A $2_0 - 1_0$	96741.38	5.5	0.472	2.39×10^{13}
E $2_{-1} - 1_{-1}$	96739.39	3.3	0.678	2.77×10^{13}
E $2_0 - 1_0$	96744.55	5.5	0.042	2.68×10^{14}

[1] $f_{\rm low}$ is the fraction of A- or E-type CH_3OH in the lower, $J = 1$, level of the transition in equilibrium with the 2.73 K background; [2] $N(\text{X-}CH_3OH) = q_X \int \tau_{2-1} dv$ for either the A- or E-state.

to having 6 antennas simultaneously observing), and the empirically-determined rms error in line/continuum ratio in the final, reduced spectra.

Six correlator bands of 20 MHz were concatenated to cover frequencies from 97 600 to 97 800 MHz (or a ∼150 km s^{-1} bandwidth) with a channel spacing of 39.06 kHz or 0.121 km s^{-1} and a channel width of 70 kHz. Two additional correlator bands of 320 MHz were used to measure the 3 mm continuum over the 580 MHz instantaneous IF-bandwidth available with this generation of receivers. The fluxes of the quasar continuum were determined relative to the primary flux calibrator used at Plateau de Bure, i.e. MWC349. The resulting flux accuracy is ∼15%.

The data were processed inside the GILDAS/CLIC software[1] (Pety 2005). After a standard RF bandpass calibration, the time-dependent amplitude and phase gains were computed per baseline on the continuum data, assuming a point source. Those gains were then applied to the line data taken simultaneously and spectra were computed as a weighted temporal average of the visibility amplitudes.

2.2. Spectroscopy and observed transitions

Rest frequencies for the CH_3OH transitions (Table 2) were taken from the NIST list of recommended rest frequencies, found online at http://physics.nist.gov/cgi-bin/micro/table5/start.pl. Although the spectroscopic constants have changed slightly, helpful energy level diagrams and related information for CH_3OH are given by Lees (1973); Nagai et al. (1979) and Friberg et al. (1988); Lees (1973) tabulates line strengths and spontaneous emission coefficients. As noted in Table 2, we observed several $J = 2_K$–1_K transitions of A- and E-type CH_3OH around 96 740 MHz. For E-CH_3OH the $J = 0$ level of the $K = -1$ ladder is absent owing to symmetry concerns and the $J = 2_{-1} - 1_{-1}$ transition is actually the ground-state E-CH_3OH line. The fourth column of Table 2 gives the fraction of all A- or E-CH_3OH which resides in the 1_K level of the various transitions when the rotational populations are in

[1] See http://www.iram.fr/IRAMFR/GILDAS for more information about the GILDAS software.

Table 3. Background sources observed in HC_5N $J = 8$–7.

Source	l °	b °	Time h	$\sigma^1_{l/c}$ $\times 10^{-3}$	$\sigma \int \tau dv^2$ 10^{-3} km s^{-1}
B0212+735	128.9	12.0	1.1	1.5	2.2
B0355+508	150.4	−1.6	1.2	1.4	2.0
B0415+379	161.7	−8.8	1.2	1.3	2.5
B2200+420	92.6	−10.4	1.1	1.6	3.2

[1] $\sigma_{l/c}$ = rms error in the line/continuum ratio; [2]$\sigma \int \tau dv$ = rms error in integrated optical depth.

equilibrium with the 2.73 K cosmic microwave background. The total column density of CH_3OH is the sum of all A- and E-CH_3OH.

According to Lees (1973), the transitions observed are all of a-type, with dipole moment of 0.885 D, leading to the spontaneous emission rates A_{21} shown in Table 2. From standard formulae, given the assumed excitation and level populations, we may write for either the $X = A$ or $X = E$ configurations $N(\text{X-}CH_3OH) = q_X \int \tau_{2-1} dv$, where the observed optical depth integral over any of the $J = 2_K$–1_K lines is expressed in km s^{-1} and values of q_X are given in the last column of Table 2.

3. Cyanopolyyne observations and data

We observed the $J = 5$–4 HC_3N and $J = 8$–7 HC_5N transitions at 45.4 and 21.3 GHz at the VLA on 2007 December 16–17 using a correlator setup with 128 channels of width 24.4 kHz and 12.2 kHz, respectively (0.161 km s^{-1} and 0.172 km s^{-1}). We bandpass calibrated and then observed the background sources fixedly without the need for other phase calibrators, given the strong emission and point-like nature of the sources (all of which are calibrators for other experiments). We used reference pointing on all sources. After applying the bandpass calibration, we used the AIPS task UVLSD which forms and averages line/continuum spectra during individual correlator integration intervals. The final spectra were then formed with vector averaging in the POSSM task and exported for reduction and analysis. The fluxes of the background sources were not needed to form the absorption spectra and were not separately determined.

Although unforseen, it has not been possible to correlate baselines with both VLA and eVLA antennas at the narrow IF bandwidths used in this work. Given the makeup of the VLA during our observations, it was necessary to discard nearly half of the the baselines. Additionally, the Q-band HC_3N observations were corrupted by an unexplained IF instability or other problem which made passband calibration problematic and rendered the noise levels several times higher than expected. Although some portions of some passbands appeared to be usable for some sources, we do not trust these results and we will not discuss them further. Results for the HC_5N transition toward four sources (those observed in CH_3OH as well as B0212+735) are summarized in Table 3.

Given the relatively large mass and high dipole moments of the cyanopolyynes, 3.6 and 4.33 Debye for HC_3N and HC_5N, respectively, maximizing the sensitivity of the detection experiment required consideration of the populations of the rotational ladder. Although the density of neutral particles is too low to produce significant departures from rotational equilibrium with the cosmic background (see Sect. 4.3), excitation by electrons is non-negligible. Figure 1 shows the integrated optical depths expected for various rotational transitions as a function

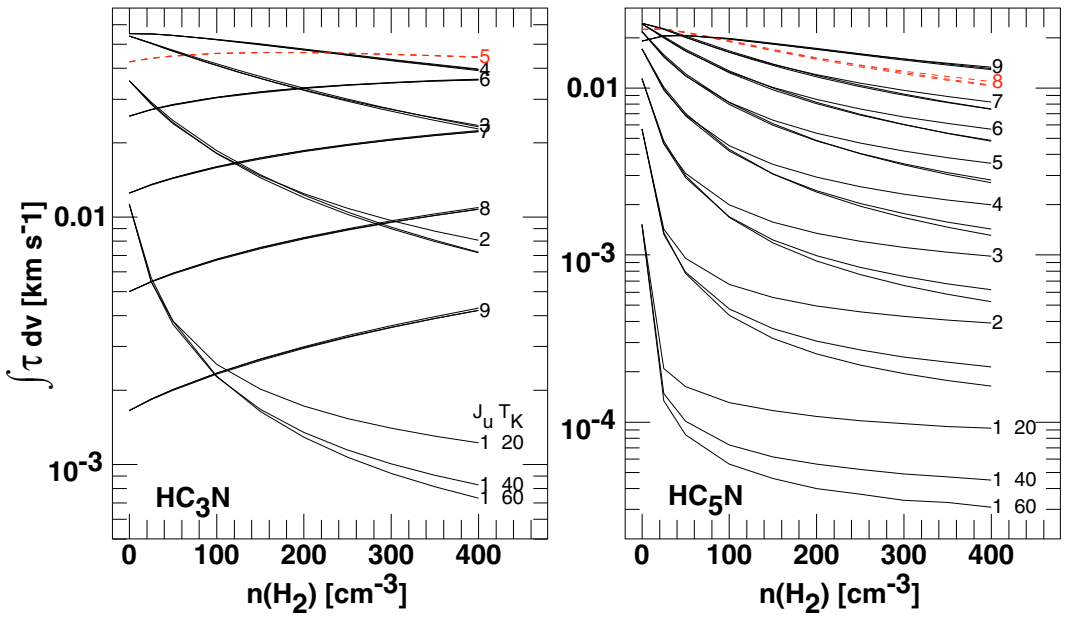

Fig. 1. Excitation of cyanopolyynes by electrons in diffuse gas. Shown are the integrated optical depths for $J_u \rightarrow J_u - 1$ transitions as a function of H_2-number density when $X(e) = n(e)/n(H_2) = 4 \times 10^{-4}$. At left are shown results for $N(HC_3N) = 10^{12}$ cm^{-2} and at right for $N(HC_5N) = 10^{12}$ cm^{-2}. For each transition, calculations at T_K = 20, 40, and 60 K are shown but only for lower-J transitions are they clearly separated. In each case the curve for the highest T_K-value lies lowest. The transitions observed in this work are shown as dashed (red) lines.

of the assumed temperature and density of molecular hydrogen, under the assumption that $n(e)/n(H_2) = 4 \times 10^{-4}$ representing a fully ionized component of moderately-depleted carbon, $n(C) = 3 \times 10^{-4} n(H_2)$, along with a smaller contribution by H^+. We solved the rate equations determining the level populations for a total column density 10^{12} cm^{-2} of absorbers, including collisional excitation by electrons using the rate constants of Dickinson & Flower (1981).

Technical details aside, the transitions having the greatest integrated optical depth are those which most sensitively probe the actual molecular abundance. The J = 5–4 HC_3N and J = 8–7 HC_5N transitions are the first or second-most sensitive transitions over the range of density indicated. The calculated optical depth of the J = 8–7 HC_5N transition is insensitive to temperature but declines slightly with increasing density. Given the behaviour shown in Fig. 1, it is conservative to assert that $\int \tau_{8-7} dv = 10^{-14}$ km s^{-1} $N(HC_5N)$ and the upper limits on the J = 8–7 line profile optical depth integrals given in Table 3 have been converted to HC_5N column density in Table 4 using this value.

4. Results and comparison with dark cloud abundances

4.1. CH_3OH

The bottom row of Table 4 gives limits on the total CH_3OH column density toward B0415+479 (3C 111) and B2200+420 (BL Lac) and for the –10.5 km s^{-1} component toward B0355+508 (NRAO150), which has the highest column densities and is chemically the most complex feature along that sightline (Liszt et al. 2006). These are 2σ statistical upper limits at the empirically-determined channel-to-channel rms levels tabulated in Table 1, over the expected velocity span determined by our deep HCO^+ profiles for each line. The features toward 3C111 and BL Lac have blended velocity substructure, but this distinction is ignored here. Spectra of the various species in the directions discussed are given in the references cited in Table 4.

Table 4 also compares these limits on the CH_3OH column density with values for the column densities of a variety of molecules previously observed toward the various features in our earlier work. To compare with dark cloud values, the right-most column of Table 4 gives the abundances of the various species seen in TMC-1.

Our upper limits on the CH_3OH column density are in all cases quite low compared to those of the other species shown in Table 4, and are generally at or modestly below the abundance ratios seen in TMC-1, especially toward 3C111. For instance $N(CH_3OH)/CS < 0.2$, 0.1, and 0.13 for BL Lac, NRAO150, and 3C111, respectively, compared with a value 0.2 toward TMC-1.

4.2. HC_5N

As noted in Sect. 3, the upper limits on the line profile integral of HC_5N absorption in Table 3 were converted to column density for inclusion in Table 4 using $N(HC_5N) = 10^{14}$ cm^{-2} $\int \tau dv$, following the excitation calculations shown in Fig. 1. The HCN/HC_5N ratio, approximately 7 in TMC-1, is at least 3–10 times higher than this toward B2200 and B0415+379.

4.3. Chemical abundances and physical conditions in diffuse clouds

Table 4 serves as a summary of our absorption line chemistry work to date, for sightlines and clouds with somewhat higher column density $N(HCO^+) > 10^{12}$ cm^{-2} which have the richest chemistry. These patterns are not universal: the abundances of CO and all other detected species listed beneath C_3H_2 in the table increase dramatically with respect to HCO^+ for $N(HCO^+) \gtrsim 10^{12}$, as shown for instance in Fig. 3 of Liszt & Lucas (2001). CO, which is found in nearly all features identified in HCO^+, even at $N(HCO^+) < 10^{12}$, is a special case, varying widely due

Table 4. Column densities and relative abundances.

Species	B2200 10^{12} cm^{-2}	B0355 10^{12} cm^{-2}	B0415 10^{12} cm^{-2}	TMC-1[6] 10^{13} cm^{-2}
OH[7]	68	34	360	300
CO[8]	1.9×10^4	0.5×10^4	$5–8 \times 10^4$	8×10^4
HCO^{+}[1]	2.0	1.2	11.6	8
C_2H[2]	31	23	75	50–100
C_3H_2[2]	5.0	3.7	13.3	10
H_2CO[3]	6.2	6.9	20.5	20
CS[4]	2.7	4.3	10.1	10
HCS^{+}[4]			0.76	0.6
SO[4]	3.43	1.66	13.0	5
H_2S[4]	0.52	0.76	1.66	<0.5
NH_3[3]		2.5	12.2	20
CN[5]	32.9	41	158	30
HCN[5]	4.5	3.6	24.8	20
HNC[5]	0.74	1.1	5.54	20
HC_5N[5]	<0.20	<0.25	<0.32	3
CH_3OH	<0.52	<0.43	<1.3	2

[1] Lucas & Liszt (1996); [2] Lucas & Liszt (2000); [3] Liszt et al. (2006); [4] Lucas & Liszt (2002); [5] Liszt & Lucas (2001); [6] Ohishi et al. (1992); [7] Liszt & Lucas (2000); [8] Liszt & Lucas (1998).

to the influence of photodissocation and self-shielding (Liszt 2007). It can however be understood as the electron recombination product of HCO^+ when $N(HCO^+)/N(H_2) = 2 \times 10^{-9}$, as observed (ibid).

Despite the overall similarity in relative abundances of many species with the TMC-1 patterns, some differences with TMC-1 are also apparent, even beyond the absence of CH_3OH and HC_5N. In particular, the low HNC/HCN ratio in diffuse clouds is characteristic of warmer gas, consistent with the observed HOC^+/HCO^+ ratio (Liszt & Lucas 2001; Liszt et al. 2004). The HCN/HNC and HOC^+/HCO^+ ratios are important clues to the diffuse nature of the host gas. Previous indications that diffuse gas was being observed were the low reddening (0.32 mag) known to exist toward B2200+420 (BL Lac), the weakness of mm-wave emission from species other than CO – only HCO^+ is detected (Liszt & Lucas 1994; Lucas & Liszt 1996) – and finding that N(OH) and N(CO) were comparable to the column densities observed in *uv* absorption toward ζ Oph and some other bright stars.

The general properties of diffuse gas are summarized by Snow & McCall (2006). In the context of our work, the kinetic temperature and the density and thermal partial pressure of H_2 are indicated in various ways by the chemistry, fractionation and rotational excitation of CO (Liszt & Lucas 1998; Liszt 2007), and are typical of the diffuse ISM. The partial thermal pressures $n(H_2)\ T_K \approx 1–5 \times 10^3$ cm^{-3} K are comparable to those derived for the bulk of the gas from C I fine-structure excitation seen in *uv* absorption (Jenkins & Tripp 2001). $N(^{12}CO)/N(^{13}CO)$ ratios may be as low as 15–20 in clouds with $N(CO) \lesssim 10^{16}$ cm^{-2}, from which it may be inferred that the kinetic temperature of lines of sight like those summarized in Table 4 is 25–50 K, somewhat below the mean kinetic temperature inferred from obsevation of H_2 itself (70–80 K, see Rachford et al. 2002) but consistent with formation and rotational excitation of CO at $n(H_2) \approx 100$ cm^{-3}. The very weak mm-wave emission of optically-thick HCO^+ is consistent with such $n(H_2)$ if $n(e)/n(H_2) \approx 4 \times 10^{-4}$ as expectedfor diffuse gas in which only a small fraction ($\lesssim$1–5%) of the free gas-phase carbon resides in CO and the rest is in the form of C^+.

Despite the consistency of these arguments, it is the case that no quiescent ion-molecule chemistry will reproduce the observed abundances at such low n(H_2). Some recent models of the diffuse cloud chemistry regard these conditions as a general background against which transient processes may operate (Falgarone et al. 2006; Smith et al. 2004), affecting the observed chemical abundance patterns without necessarily imprinting themselves observably on the internal degrees of freedom in the molecules themselves.

Acknowledgements. IRAM is supported by INSU/CNRS (France), MPG (Germany), and IGN (Spain). The National Radio Astronomy Observatory is operated by AUI, Inc. under a cooperative agreement with the US National Science Foundation. We owe the staff at IRAM (Grenoble) and the Plateau de Bure our thanks for their assistance in taking the data. We thank the scientific staff at the VLA, especially Mark Claussen, for assistance in dealing with data-handling issues during the VLA/eVLA transition. The referee provided a gentle but perceptive report which resulted in great improvement of the text. We thank Maryvonne Gerin for encouraging us to search for CH_3OH.

References

Dickinson, A. S., & Flower, D. R. 1981, MNRAS, 196, 297
Falgarone, E., Pineau Des Forêts, G., Hily-Blant, P., & Schilke, P. 2006, A&A, 452, 511
Friberg, P., Hjalmarson, A., Madden, S. C., & Irvine, W. M. 1988, A&A, 195, 281
Jenkins, E. B., & Tripp, T. M. 2001, A&AS, 137, 297
Lees, R. M. 1973, ApJ, 184, 763
Liszt, H. S. 2007, A&A, 476, 291
Liszt, H. S., & Lucas, R. 1994, ApJ, 431, L131
Liszt, H. S., & Lucas, R. 1995, A&A, 299, 847
Liszt, H. S., & Lucas, R. 1998, A&A, 339, 561
Liszt, H. S., & Lucas, R. 2000, A&A, 355, 333
Liszt, H., & Lucas, R. 2001, A&A, 370, 576
Liszt, H., Lucas, R., & Black, J. H. 2004, A&A, 428, 117
Liszt, H., Lucas, R., & Pety, J. 2006, A&A, 448, 253
Lucas, R., & Liszt, H. S. 1996, A&A, 307, 237
Lucas, R., & Liszt, H. S. 2000, A&A, 358, 1069
Lucas, R., & Liszt, H. S. 2002, A&A, 384, 1054
Nagai, T., Kaifu, N., Nagane, K., & Akaba, K. 1979, Publ. Astron. Soc. Jpn., 31, 317
Nash, A. G. 1990, A&ASS, 72, 303
Ohishi, M., Irvine, W., & Kaifu, N. 1992, in Astrochemistry of cosmic phenomena, Proc. 150th Symp. Inter. Astro. Union, ed. P. D. Singh, held at Campos do Jordao, Sao Paulo, Brazil, August 5–9, 1991 (Dordrecht: Kluwer), 171
Pety, J. 2005, in Semaine de l'Astrophysique Française, ed. F. Casoli, T. Contini, J. M. Hameury, & L. Pagani, SF2A-2005, 721
Price, R. J., Viti, S., & Williams, D. A. 2003, Mon. Not. R. Astron. Soc., 343, 1257
Rachford, B. L., Snow, T. P., Tumlinson, J., et al. 2002, ApJ, 577, 221
Smith, M. D., Pavlovski, G., MacLow, M.-M., et al. 2004, Ap&SS, 289, 333
Snow, T. P., & McCall, B. J. 2006, ARA&A, 44, 367
Viti, S., Williams, D. A., & O'Neill, P. T. 2000, A&A, 354, 1062